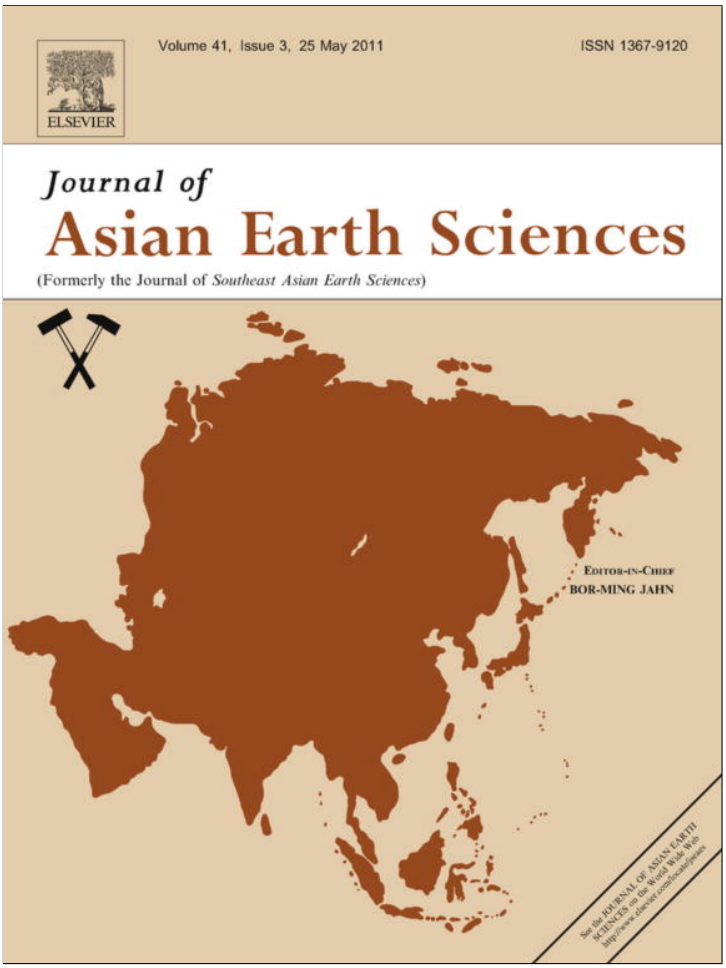

Journal of Asian Earth Sciences 41 (2011) 344–354

Contents lists available at ScienceDirect

Journal of Asian Earth Sciences

journal homepage: www.elsevier.com/locate/jseaes

# Depositional provenance of the Greater Himalayan Sequence, Garhwal Himalaya, India: Implications for tectonic setting

Christopher J. Spencer [a,*], Ron A. Harris [a], Himanshu Kumar Sachan [b], Anubhooti Saxena [b]

[a] Dept. of Geological Sciences, Brigham Young University, Provo, UT, USA
[b] Wadia Institute of Himalayan Geology, Dehra Dun 248 001, India

ARTICLE INFO

*Article history:*
Received 6 July 2010
Received in revised form 28 December 2010
Accepted 9 February 2011
Available online 24 February 2011

*Keywords:*
Geochemistry
Provenance
Himalayan orogen
Greater Himalayan Sequence

ABSTRACT

The Greater Himalayan Sequence in the Garhwal Region of India is a 14–20 km thick succession of various pelitic and psammitic metasediments which contain individual units that are traceable for at least 250 km along the strike of the Himalayan range in northwestern India. Bulk rock geochemical analyses show a chemical index of alteration (CIA) values of 57–93 with an average of 67, average $(La/Yb)_N = 18.6$, average $(La/Sm)_N = 3.7$, Cr/Th range between 0.2 and 214.5, and Th/Sc range between 0.2 and 10.3. The various geochemical tectonic indicators reveal a signature akin to an active continental margin. A low degree of weathering and high concentrations of incompatible/compatible element ratios respectively point to a proximal and primarily a silicic source region. The occurrence of three-phase halite bearing primary fluid inclusions in the quartz grains of metasediments indicate their provenance from a magmatic terrain. Potential source regions of the Greater Himalayan Sequence are the East African Orogeny, the East Antarctic Orogeny, and/or the Bhimpedian Orogeny of Northern India.

Fluid inclusions in the Greater Himalayan Sequence (three-phase halite bearing inclusions, moderately high temperature bi-aqueous inclusions, and carbonic-aqueous inclusions) estimate maximum salinity at ~33 wt.% NaCl. This occurrence of fluid inclusions is also consistent with a magmatic terrain.



## 1. Introduction

The provenance of the Greater Himalayan Sequence is a persistent question for reconstructions of the Himalayan orogen has been the focus of several different studies (Parrish and Hodges, 1996; Ahmad et al., 2000; DeCelles et al., 2000; Upreti and Yoshida, 2005; Yin, 2006; Yoshida and Upreti, 2006; Imayama and Arita, 2007). These previous investigators have used isotopic compositions and detrital zircon U–Pb ages to constrain the provenance. However, none of these studies have used bulk rock chemistry to substantiate their findings and to identify the depositional setting of the Greater Himalayan Sequence. In this paper, we report bulk-rock major, trace, and rare earth element of the various units within the Greater Himalayan Sequence, Garhwal Himalayas (Figs. 1 and 2).

In the Garhwal Himalaya, the Greater Himalayan Sequence is a 14–20 km thick succession of metapelites and metapsammites with three major units: the Joshimath, Pandukeshwar, and Badrinath formations. The Greater Himalayan Sequence is bounded at the base by the Vaikrita thrust, which places the high grade Greater Himalayan Sequence on top of the low grade Lesser Himalayan Sequence; and bounded at the top by the Southern Tibetan Detachment, which juxtaposes the unmetamorphosed Tethyan Himalayan Sequence next to the Greater Himalayan Sequence. Within the Greater Himalayan Sequence the contacts are purely depositional grading from the primarily metapelitic Joshimath formation at the base, to the arkose quartzitic Pandukeshwar formation, to the metapelitic Badrinath formation at the top. Within the Chamoli district (Uttarakhand, India) the metasediments of the Greater Himalayan Sequence are 4–10 times thicker (14–20 km) than anywhere else in the Western Himalaya (Virdi, 1986; Paul, 1998; Valdiya et al., 1999). The Greater Himalayan Sequence has reportedly undergone three major phases of deformation and metamorphism: Paleozoic-age compression, Cenozoic-age compression, and most recently Miocene-age extension and exhumation (Virdi, 1986; Gairola and Srivastava, 1987; Gururajan and Choudhuri, 1999). These deformational events have caused an indeterminable amount of ductile thickening and shortening. Mesoscale isoclinal and recumbent, rootless folds deform the Greater Himalayan Sequence throughout the region studied.

Various models have been introduced to explain the provenance of the Greater Himalayan Sequence. The most prominent of the models are the single margin model, active continental margin model, and rift basin model (see Yin, 2006 for a review of these models).

* Corresponding author.
*E-mail address:* chrisspencer@byu.edu (C.J. Spencer).

1367-9120/$ - see front matter © 2011 Elsevier Ltd. All rights reserved.
doi:10.1016/j.jseaes.2011.02.001

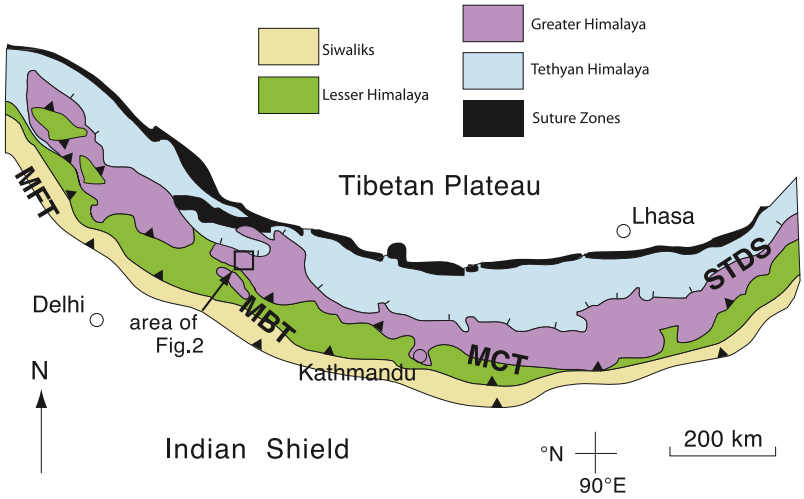


**Fig. 1.** Generalized tectonic map of the Himalayan orogen (after Ahmad et al., 2000; Thakur and Rawat, 1992). Major fault systems include the South Tibetan detachment system (STDS), the Main Central or Vaikrita thrust (MCT), the Main Boundary thrust system (MBT), and the Main Frontal thrust system (MFT).

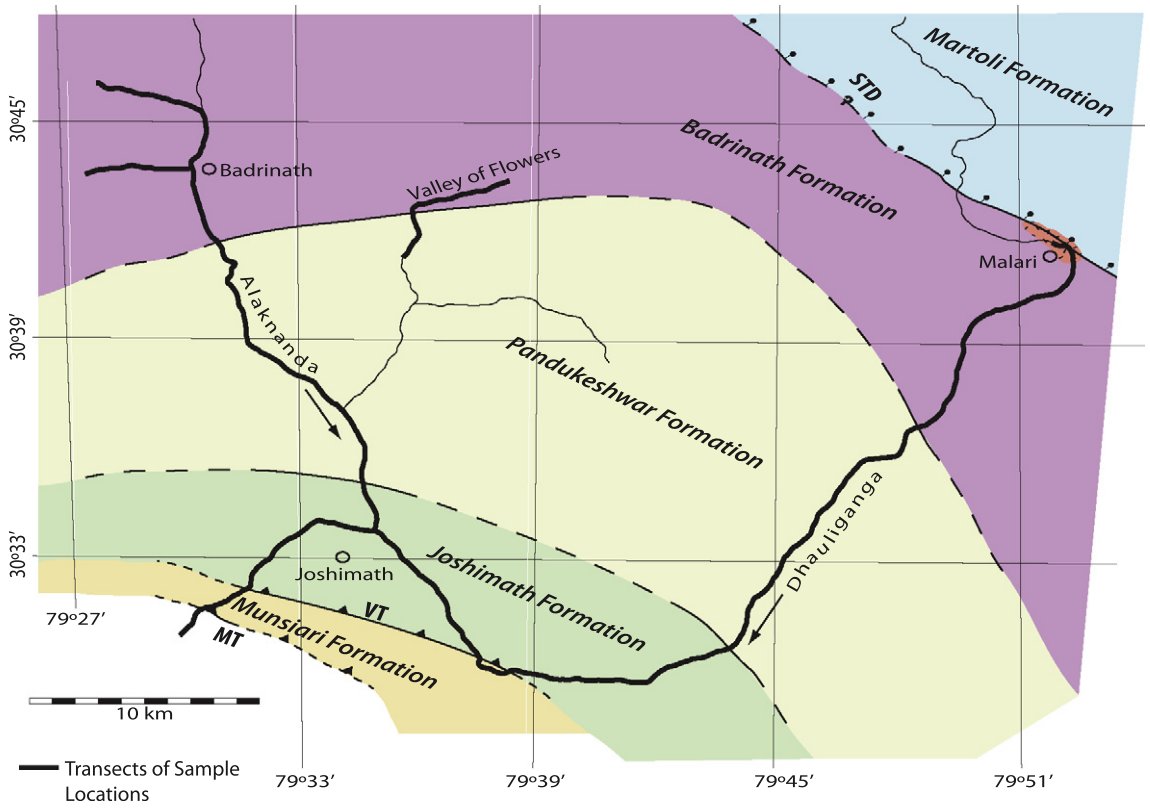


**Fig. 2.** Geologic map of Alaknanda/Dhauliganga section of the Garhwal Himalaya showing sample locations. STD – South Tibetan Detachment, VT – Vaikrita thrust, MT – Munsiari thrust.

## 2. Analytical methods

Bulk-rock major and selected trace element X-ray florescence (XRF) analyses were conducted on 49 samples for major elements and 42 samples for trace elements with a Siemens SRS 303 at Brigham Young University. Additional trace elements and rare earth elements were determined for 54 samples by inductively coupled plasma mass spectrometry (ICP-MS) at ALS Chemex laboratories, Vancouver (method ME-MS81) and the Wadia Institute of Himalayan Geology. Samples used for XRF analysis were crushed using a tungsten carbide shatterbox in order to avoid Cr contamination.

## 3. Bulk-rock analyses

Bulk-rock major, trace, and rare earth element analyses and sample locations of metasedimentary units of the Greater Himalayan Sequence are presented in Tables 1a–1c and Fig. 2, respectively. Due to the high grade metamorphism of the Greater Himalayan Sequence it is important to determine the mobility of the various elements measured to ascertain how well the measured concentrations represent the initial compositions of the proto-Greater Himalayan Sequence. Cullers et al. (1997) have shown that most major and trace element abundances remain constant

**Table 1a**
Selected major element analyses.

| Sample | Formation | $Na_2O$ | MgO | $Al_2O_3$ | $SiO_2$ | $P_2O_5$ | $K_2O$ | CaO | $TiO_2$ | MnO | $Fe_2O_3$ | L.O.I. | Total | CIA |
|---|---|---|---|---|---|---|---|---|---|---|---|---|---|---|
| GH12 | Joshimath | 2.22 | 2.07 | 14.84 | 69.97 | 0.13 | 4.02 | 1.00 | 0.36 | 0.04 | 3.73 | 1.02 | 99.40 | 67.21 |
| GH14 | | 0.25 | 1.89 | 16.34 | 63.20 | 0.14 | 3.95 | 1.76 | 1.11 | 0.18 | 8.24 | 1.99 | 99.03 | 73.29 |
| GH16 | | 1.98 | 3.16 | 14.72 | 66.33 | 0.15 | 4.03 | 1.12 | 0.79 | 0.07 | 5.72 | 2.02 | 100.09 | 67.37 |
| GH17 | | 1.25 | 2.03 | 10.26 | 77.67 | 0.12 | 2.47 | 1.70 | 0.58 | 0.07 | 4.52 | 0.93 | 101.58 | 65.44 |
| GH34 | | 0.09 | 6.18 | 3.20 | 89.31 | 0.01 | 0.02 | 0.12 | 0.09 | 0.01 | 1.92 | 1.03 | 101.98 | 93.29 |
| GH37 | | 2.79 | 1.31 | 15.05 | 67.65 | 0.15 | 3.61 | 1.21 | 0.58 | 0.05 | 4.93 | 2.02 | 99.35 | 66.42 |
| GH38 | | 0.16 | 0.35 | 5.34 | 88.04 | 0.21 | 1.57 | 0.31 | 2.63 | 0.01 | 2.03 | 1.01 | 101.66 | 72.36 |
| GH39 | | 1.16 | 3.48 | 26.72 | 48.74 | 0.04 | 8.62 | 0.60 | 1.14 | 0.07 | 6.43 | 3.00 | 100.00 | 72.02 |
| GH40 | | 2.53 | 2.74 | 14.04 | 70.23 | 0.13 | 2.75 | 1.36 | 0.66 | 0.04 | 4.31 | 2.02 | 100.81 | 67.89 |
| GH61 | | 1.15 | 1.91 | 15.72 | 65.87 | 0.14 | 3.43 | 1.28 | 0.76 | 0.13 | 6.81 | 1.27 | 98.47 | 72.82 |
| AS68B | | 3.22 | 0.35 | 15.35 | 72.71 | 0.31 | 4.91 | 0.74 | 0.17 | 0.02 | 1.98 | | 99.75 | 63.39 |
| AS69A | | 2.48 | 0.94 | 18.63 | 67.54 | 0.08 | 3.79 | 0.43 | 0.56 | 0.12 | 4.64 | | 99.23 | 73.51 |
| GH22 | Pandukeshwar | 0.31 | 0.45 | 12.88 | 77.28 | 0.01 | 3.27 | 0.13 | 0.61 | 0.09 | 4.07 | 1.01 | 100.11 | 77.64 |
| GH24 | | 1.52 | 0.51 | 4.84 | 88.20 | 0.10 | 1.25 | 0.92 | 0.36 | 0.04 | 2.19 | 1.01 | 100.94 | 56.74 |
| GH26 | | 0.21 | 0.64 | 10.00 | 80.18 | 0.04 | 4.33 | 0.81 | 0.36 | 0.10 | 3.44 | 1.01 | 101.12 | 65.15 |
| GH27 | | 1.74 | 0.45 | 4.89 | 90.92 | 0.05 | 0.66 | 0.54 | 0.24 | 0.03 | 1.65 | 0.12 | 101.28 | 62.46 |
| GH44 | | 0.12 | 0.28 | 5.17 | 90.96 | 0.02 | 2.03 | 0.16 | 0.20 | 0.02 | 1.34 | 1.01 | 101.31 | 69.12 |
| GH47 | | 0.86 | 1.64 | 16.63 | 64.08 | 0.08 | 5.91 | 0.58 | 0.87 | 0.08 | 5.91 | 3.03 | 99.67 | 69.35 |
| GH47b | | 0.44 | 1.47 | 15.45 | 67.66 | 0.06 | 5.67 | 0.53 | 0.75 | 0.08 | 5.32 | 1.69 | 99.11 | 69.96 |
| AS54A | | 0.01 | 0.03 | 1.92 | 95.72 | 0.06 | 0.27 | 0.15 | 0.12 | 0.01 | 0.97 | | 99.25 | 81.84 |
| AS55A | | 0.09 | 1.19 | 4.52 | 90.21 | 0.14 | 1.16 | 0.58 | 0.16 | 0.02 | 2.28 | | 100.35 | 71.20 |
| AS65A | | 1.71 | 0.52 | 8.16 | 82.79 | 0.08 | 3.30 | 0.37 | 0.36 | 0.02 | 3.59 | | 100.90 | 60.27 |
| AS67A | | 4.24 | 0.46 | 7.29 | 85.92 | 0.08 | 0.19 | 0.26 | 0.19 | 0.02 | 2.04 | | 100.69 | 60.85 |
| AS70A | | 2.60 | 0.77 | 9.73 | 78.49 | 0.11 | 0.71 | 3.05 | 0.68 | 0.12 | 4.73 | | 101.00 | 60.46 |
| AS71A | | 0.99 | 0.29 | 5.23 | 89.91 | 0.08 | 0.94 | 0.62 | 0.33 | 0.04 | 1.96 | | 100.39 | 67.19 |
| AS71B | | 0.28 | 0.63 | 12.04 | 78.01 | 0.12 | 3.67 | 0.24 | 0.45 | 0.05 | 3.56 | | 99.05 | 74.19 |
| AS72A | | 0.29 | 0.27 | 6.37 | 88.78 | 0.07 | 1.78 | 0.21 | 0.31 | 0.06 | 2.20 | | 100.34 | 73.66 |
| AS72C | | 0.44 | 0.32 | 6.98 | 87.58 | 0.14 | 2.41 | 0.26 | 0.24 | 0.04 | 2.48 | | 100.89 | 69.15 |
| AS75A | | 0.54 | 0.11 | 4.15 | 92.23 | 0.09 | 1.70 | 0.39 | 0.11 | 0.02 | 1.28 | | 100.63 | 61.18 |
| AS76A | | 1.30 | 0.22 | 5.84 | 88.89 | 0.11 | 1.70 | 0.58 | 0.18 | 0.02 | 1.58 | | 100.41 | 62.04 |
| AS76B | | 1.05 | 0.20 | 5.76 | 88.14 | 0.12 | 2.00 | 0.64 | 0.48 | 0.06 | 2.29 | | 100.76 | 60.90 |
| AS76C | | 1.60 | 0.15 | 4.90 | 90.71 | 0.11 | 1.07 | 0.31 | 0.19 | 0.02 | 1.31 | | 100.37 | 62.21 |
| AS77A | | 1.31 | 0.16 | 5.95 | 88.19 | 0.12 | 2.05 | 0.54 | 0.24 | 0.04 | 1.84 | | 100.43 | 60.42 |
| AS78A | | 0.48 | 0.24 | 6.28 | 84.79 | 0.11 | 2.58 | 0.42 | 0.14 | 0.02 | 1.84 | | 96.90 | 64.37 |
| AS79A | | 0.75 | 0.11 | 4.13 | 91.72 | 0.11 | 1.46 | 0.46 | 0.11 | 0.02 | 1.20 | | 100.06 | 60.74 |
| AS81A | | 0.12 | 0.28 | 4.98 | 90.56 | 0.11 | 1.74 | 0.34 | 0.14 | 0.03 | 1.85 | | 100.16 | 69.41 |
| AS81B | | 0.06 | 0.32 | 5.56 | 90.31 | 0.12 | 1.85 | 0.25 | 0.17 | 0.03 | 1.88 | | 100.58 | 71.96 |
| AS82A | | 0.61 | 0.10 | 3.98 | 92.01 | 0.16 | 1.77 | 0.47 | 0.07 | 0.03 | 1.19 | | 100.38 | 58.28 |
| AS83A | | 0.45 | 0.05 | 2.88 | 93.59 | 0.11 | 1.18 | 0.33 | 0.12 | 0.02 | 1.15 | | 99.86 | 59.54 |
| AS84A | | 0.41 | 0.10 | 3.10 | 93.11 | 0.12 | 1.09 | 0.36 | 0.20 | 0.02 | 1.63 | | 100.14 | 62.46 |
| AS85A | | 0.64 | 0.12 | 3.93 | 92.22 | 0.12 | 1.32 | 0.36 | 0.11 | 0.05 | 1.33 | | 100.21 | 62.88 |
| GH29 | Badrinath | 2.98 | 2.48 | 16.54 | 61.57 | 0.05 | 4.68 | 1.12 | 0.89 | 0.10 | 6.86 | 2.02 | 99.29 | 65.32 |
| GH32 | | 4.12 | 0.91 | 16.91 | 66.64 | 0.12 | 5.62 | 1.18 | 0.39 | 0.02 | 2.74 | 0.60 | 99.25 | 60.76 |
| GH33 | | 2.39 | 2.31 | 17.63 | 62.45 | 0.13 | 5.67 | 0.74 | 0.88 | 0.05 | 5.39 | 3.03 | 100.67 | 66.70 |
| GH33b | | 3.84 | 1.84 | 10.98 | 74.51 | 0.16 | 0.98 | 1.56 | 0.67 | 0.09 | 5.46 | 1.01 | 101.10 | 63.25 |
| GH52 | | 1.02 | 0.32 | 5.16 | 88.20 | 0.02 | 0.20 | 1.90 | 0.25 | 0.19 | 2.67 | 1.03 | 100.96 | 62.32 |
| GH54 | | 0.67 | 1.56 | 16.63 | 63.66 | 0.06 | 4.81 | 0.55 | 0.94 | 0.11 | 7.36 | 3.04 | 99.39 | 73.39 |

relative to $Al_2O_3$. However, Masters and Ague (2005) demonstrate that Al mobility is possible during regional metamorphism. Cullers et al. (1997) and Masters and Ague (2005) also suggest that no mobilization of the elements of interest (REE, Th, Sc, Co, and Cr). Pearce and Cann (1971, 1973) also determined that the elements Zr, Y, Nb and Cr are generally immobile during alteration up through greenschist facies metamorphism. Zr has also been shown to be particularly immobile (Masters and Ague, 2005). Sr (Pearce and Cann, 1973), P (Winchester and Floyd, 1976), K (Pearce et al., 1975), Mg, Br, and Na (Pearce, 1996), Ti (Ague, 2003) have been shown to be more mobile during alteration and metamorphic processes, thus tectonic discrimination diagrams that use these mobile elements were avoided. Within the Greater Himalayan Sequence in Sikkim, Dasgupta et al. (2009) showed there to be a general mass gain for $SiO_2$ and a low overall mobility of elements with only occasional exceptions within the Greater Himalayan Sequence.

In addition to metasomatism and metamorphic reactions, the composition of metamorphic rocks can also vary due to chemical weathering which may be imprinted in the sedimentary record (Nesbitt and Young, 1982; McLennan et al., 1993; Li et al., 2005). This tool can be used to identify intensity of chemical weathering and potential source areas. The most widely used chemical index to quantitatively measure the intensity of chemical weathering is the chemical index of alteration (CIA) as proposed by Nesbitt and Young (1982). CIA is calculated by the following equation: $CIA = Al_2O_3/(Al_2O_3 + CaO + Na_2O + K_2O) \times 100$. Unweathered igneous rocks have CIA values of 50 or less, whereas intense weathering, which results in residual clay with high kaolinite produces CIA values close to 100 (Li et al., 2005). CIA values for Greater Himalayan Sequence metasedimentary samples range from 57 to 93 with an average of 67, thus showing a relatively moderate degree of weathering (Fig. 3a). Low CIA values, $(La/Yb)_N$ and $(La/Sm)_N$ ratios (Table 1) display a local, juvenile crustal source, suggesting high erosion rates, little transport, poor sorting, and rapid deposition of the sediments (Camiré et al., 1993; Gao and Wedepohl, 1995). High Cr values (500–870 ppm) in several samples throughout the Greater Himalayan Sequence and the presence detrital chromite are also indicative of an active continental margin with a mafic component (McLennan et al., 1993; Hofmann, 2005; Al-Juboury et al., 2009).

Cr/Th vs Th/Sc (Fig. 3b) discriminates various sediments derived from different tectonic settings (Bracciali et al., 2007). Sediments

**Table 1b**
Selected XRF trace element analyses.

| Sample | Formation | Ba | Co | Cr | Cu | Ga | Nb | Nd | Ni | Pb | Rb | Sc | Sm | Sr | Y | Zn | Zr |
|---|---|---|---|---|---|---|---|---|---|---|---|---|---|---|---|---|---|
| GH12 | Joshimath | 409.2 | 11.4 | 14.8 | 10.1 | 25.1 | 12.3 | 31.3 | 1.8 | 27.3 | 228.2 | 13.8 | 5.3 | 81.9 | 25.6 | 37.6 | 147.3 |
| GH14 | | 663.3 | 15.8 | 543.1 | 36.9 | 20.8 | 12.5 | 24.7 | 26.2 | 46.6 | 177.9 | 4.4 | 4.8 | 40.4 | 25.9 | 175.4 | 219.3 |
| GH16 | | 525.1 | 14.9 | 86.0 | 33.2 | 22.4 | 7.6 | 24.1 | 38.3 | 19.5 | 133.5 | 21.7 | 5.1 | 94.5 | 23.5 | 61.9 | 150.7 |
| GH17 | | 515.6 | 15.3 | 81.9 | 31.1 | 22.3 | 8.5 | 22.8 | 37.6 | 18.7 | 136.4 | 21.9 | 4.7 | 96.5 | 24.4 | 61.7 | 159.8 |
| GH20 | | 547.5 | 9.2 | 623.6 | 43.4 | 13.4 | 8.6 | 20.6 | 41.0 | 19.6 | 107.6 | 0.0 | 4.4 | 105.2 | 30.6 | 57.0 | 197.2 |
| GH34 | | 668.7 | 13.4 | 83.5 | 15.5 | 23.8 | 12.3 | 34.0 | 40.0 | 25.2 | 241.5 | 11.1 | 7.0 | 146.3 | 19.7 | 60.1 | 188.3 |
| GH35 | | 570.1 | 15.5 | 356.1 | 28.9 | 17.3 | 15.1 | 30.7 | 43.4 | 31.7 | 139.7 | 11.9 | 5.0 | 129.0 | 35.3 | 88.0 | 200.0 |
| GH36 | | 590.2 | 11.3 | 361.1 | 31.9 | 17.2 | 12.2 | 27.3 | 46.2 | 31.4 | 139.8 | 0.0 | 6.5 | 126.9 | 31.7 | 85.0 | 185.7 |
| GH37 | | 285.4 | 54.2 | 382.1 | 23.2 | 21.5 | 10.9 | 25.7 | 52.8 | 10.4 | 36.1 | 0.0 | 2.4 | 272.0 | 26.4 | 120.8 | 135.3 |
| GH38 | | 604.4 | 12.2 | 26.5 | 19.5 | 24.1 | 15.9 | 42.3 | 4.0 | 78.3 | 162.9 | 14.1 | 7.8 | 76.0 | 35.2 | 175.4 | 179.3 |
| GH39 | | 16.3 | 0.8 | 19.5 | 2.4 | 14.7 | 112.9 | 46.9 | 3.8 | 27.1 | 56.7 | 0.0 | 18.8 | 6.1 | 121.0 | 36.7 | 1939.1 |
| GH40 | | 1812.1 | 10.7 | 146.8 | 0.0 | 39.3 | 3.9 | 18.4 | 13.8 | 23.1 | 281.8 | 3.7 | 0.9 | 71.5 | 9.0 | 45.6 | 253.6 |
| GH61 | | 742.7 | 14.4 | 772.1 | 23.9 | 20.7 | 12.6 | 20.6 | 42.7 | 26.2 | 190.2 | 5.2 | 4.4 | 112.1 | 28.1 | 93.6 | 209.7 |
| GH22 | Pandukeshwar | 349.8 | 5.4 | 656.8 | 12.2 | 11.5 | 7.9 | 21.0 | 35.1 | 21.8 | 74.0 | 9.2 | 3.9 | 91.7 | 34.1 | 42.7 | 257.7 |
| GH23 | | 432.8 | 0.0 | 591.9 | 4.7 | 5.7 | 0.0 | 11.7 | 20.6 | 23.8 | 64.4 | 5.4 | 4.6 | 42.2 | 20.6 | 19.6 | 90.6 |
| GH24 | | 447.5 | 0.0 | 597.4 | 6.0 | 6.2 | 0.0 | 12.0 | 19.8 | 22.9 | 63.0 | 0.0 | 4.2 | 41.0 | 20.0 | 18.8 | 88.1 |
| GH26 | | 179.5 | 13.3 | 21.4 | 33.6 | 25.7 | 0.0 | 10.3 | 0.0 | 6.4 | 14.7 | 104.1 | 5.3 | 45.1 | 12.7 | 0.0 | 87.4 |
| GH27 | | 657.0 | 5.8 | 40.6 | 11.7 | 14.4 | 3.6 | 19.7 | 15.9 | 18.9 | 129.1 | 22.1 | 5.0 | 73.3 | 20.0 | 33.5 | 160.2 |
| GH44 | | 277.8 | 6.4 | 584.3 | 26.8 | 15.8 | 11.7 | 23.2 | 31.2 | 24.3 | 139.2 | 0.0 | 5.4 | 101.8 | 27.7 | 43.6 | 202.4 |
| GH47 | | 648.7 | 13.9 | 66.9 | 14.1 | 24.0 | 14.9 | 33.4 | 27.5 | 27.8 | 216.0 | 0.0 | 5.0 | 62.9 | 40.7 | 72.5 | 340.5 |
| GH47b | | 1120.3 | 11.2 | 335.5 | 2.1 | 18.9 | 11.2 | 32.9 | 37.3 | 24.2 | 233.5 | 3.5 | 5.0 | 89.4 | 30.3 | 77.0 | 299.5 |
| GH50 | | 631.1 | 1.7 | 541.3 | 3.6 | 11.4 | 9.3 | 26.3 | 26.8 | 18.3 | 127.3 | 0.0 | 4.6 | 65.1 | 23.1 | 29.0 | 240.9 |
| GH63b | | 384.0 | 44.5 | 868.6 | 6.7 | 12.4 | 24.2 | 45.2 | 12.0 | 48.8 | 46.5 | 21.4 | 36.9 | 440.4 | 63.0 | 44.3 | 217.3 |
| GHBn1 | Badrinath | 666.7 | 19.3 | 76.0 | 60.4 | 29.3 | 17.2 | 31.7 | 38.0 | 25.9 | 181.2 | 8.4 | 6.0 | 52.9 | 26.5 | 106.6 | 221.2 |
| GH29 | | 141.6 | 0.0 | 493.3 | 7.5 | 6.7 | 3.5 | 14.0 | 27.8 | 12.3 | 33.4 | 8.0 | 4.0 | 95.1 | 19.1 | 20.3 | 157.9 |
| GH31 | | 298.6 | 21.2 | 100.0 | 9.4 | 24.8 | 19.0 | 25.3 | 49.8 | 32.0 | 300.0 | 10.8 | 4.6 | 109.5 | 22.2 | 107.3 | 146.5 |
| GH32 | | 1263.9 | 1.5 | 185.5 | 0.0 | 18.3 | 4.3 | 26.8 | 12.8 | 77.7 | 231.5 | 2.6 | 3.3 | 242.5 | 19.0 | 37.5 | 123.5 |
| GH33 | | 1264.6 | 2.3 | 186.8 | 0.0 | 18.8 | 3.9 | 24.5 | 13.8 | 76.9 | 230.0 | 2.8 | 2.6 | 241.5 | 18.8 | 35.8 | 119.7 |
| GH33b | | 269.8 | 14.9 | 74.2 | 19.0 | 21.0 | 3.8 | 22.6 | 31.5 | 14.4 | 31.9 | 30.0 | 6.8 | 102.9 | 26.0 | 45.3 | 141.7 |
| GH52 | | 58.6 | 15.9 | 28.8 | 21.5 | 21.8 | 3.6 | 17.0 | 0.0 | 0.0 | 11.3 | 70.7 | 9.0 | 72.4 | 25.4 | 1.6 | 124.6 |
| GH54 | | 698.3 | 13.4 | 66.1 | 33.0 | 25.4 | 11.4 | 33.2 | 26.9 | 25.7 | 218.5 | 9.8 | 5.8 | 72.6 | 31.6 | 83.6 | 262.6 |
| GH66 | | 493.9 | 7.5 | 336.4 | 9.8 | 20.1 | 12.0 | 24.8 | 20.1 | 40.4 | 295.1 | 2.7 | 2.9 | 85.9 | 16.5 | 78.5 | 174.4 |

with higher Cr/Th values and lower Th/Sc are indicative of more primitive sources (islands arc), and conversely lower Cr/Th values and higher Th/Sc values come from more mature sources (passive margin) with continental arcs and active continental margins lie along mixing trends between the two end members. The metasedimentary samples of the Greater Himalayan Sequence displays a wide range of values (Cr/Th = 0.2–214.5 and Th/Sc = 0.2–10.3) which shows a mixed source and potentially an active continental margin. Within the La vs Th diagram, the Greater Himalayan Sequence fall primarily in the ocean island basalt and continental arc fields (Fig. 3c). This is in accordance with the ternary diagram La–Th–Sc (Fig. 3d). In the ternary diagram V–Ni–Th * 10 (Fig. 3e), fields representative of ultramafic, mafic, and felsic rocks plot separately in roughly the three corners of the ternary plot (Bracciali et al., 2007). The Greater Himalayan Sequence samples plot dominantly in near the felsic field with a distinct mixing trend towards a mafic composition. High Cr concentrations and, together with increased MgO and $Fe_2O_3$ contents and low high field strength element contents, suggest a significant mafic to ultramafic(?) component in the source.

The REE ratios of these rocks are highly fractionated with average $(La/Yb)_N = 18.6$ (Fig. 4). The LREE are also highly fractionated with average $(La/Sm)_N = 3.8$. The La/Yb ratio (La, a light REE, is a highly incompatible element, and Yb, a heavy REE, is a less incompatible element; both are relatively immobile elements) is an excellent indicator of degree of enrichment (high value of $(La/Yb)_N$ for enriched sources) or degree of melting (lower value of $(La/Yb)_N$ for higher degree of melting) of mantle sources (Verma, 2002). Similarly, the $(La/Sm)_N$ ratio is also an indicator of mantle sources and their degree of partial melting (Verma, 2006). These features suggest that the original source areas were composed chiefly of silicic components (Li et al., 2005) and the negative Eu anomaly is evidence of a differentiated felsic source (Slack and Stevens, 1994).

## 4. Fluid inclusions

Analysis of fluid inclusions in the quartzose metasediments of the Greater Himalayan Sequence indicate the presence of high salinity three-phase aqueous inclusions (25 wt.% eq. NaCl) (Fig. 5). These fluid inclusions yield homogenization temperatures between 225 and 238 °C (Table 2). The high saline, high temperature brine inclusions probably represent granite or magmatic fluids (Cathelineau et al., 1988; De Vivo et al., 1991; Roedder, 1992). The saline aqueous three-phase inclusions as remnants of a granitic/metamorphic protolith are quite plausible. Their homogenization temperatures are however low, and may indicate a veining stage in the formation of the rocks of the protolith. Hence, a primary fluid in detrital grains is indicative of a granitic or metamorphic source.

## 5. Isotopic and geochronological provenance studies

Nd isotopes show that the Munsiari Formation of the Lesser Himalayan Sequence has a distinct isotopic signature from that of the Greater and Tethyan Himalayan Sequences. The Lesser Himalayan Sequence has an average epsilon Nd values of −22 and the Greater and Tethyan Himalayan Sequences have average values of −14 (Parrish and Hodges, 1996; Ahmad et al., 2000; Robinson et al., 2001; Richards et al., 2005; Imayama and Arita, 2007; Murphy, 2007). The epsilon Nd values in the Greater Himalayan Sequence reveal that this package of rock is more juvenile than that of the Indian craton, which indicates that it is not Indian basement (Robinson et al., 2001). These data provide support for previous interpretations that the Greater Himalayan Sequence is derived from an active continental margin which was accreted onto India during the Early Paleozoic (DeCelles et al., 2000).

Epsilon Nd values as the Greater Himalayan Sequence (average of −13) are similar to three different Proterozoic terranes from the

**Table 1c**
Selected ICP-MS trace element and rare earth analyses.

| Sample | Formation | La | Ce | Pr | Nd | Sm | Eu | Gd | Tb | Dy | Ho | Er | Tm | Yb | Lu | Sc | Y | Th | V | U |
|---|---|---|---|---|---|---|---|---|---|---|---|---|---|---|---|---|---|---|---|---|
| GH12 | Joshimath | 64.7 | 132.0 | 13.8 | 53.8 | 10.1 | 0.9 | 7.7 | 1.3 | 5.9 | 0.9 | 2.1 | 0.3 | 2.0 | 0.3 | 5.0 | 37.0 | 25.0 | 5.0 | 9.0 |
| GH14 | | 14.2 | 28.7 | 3.2 | 12.6 | 2.4 | 0.5 | 2.0 | 0.3 | 1.7 | 0.3 | 0.8 | 0.1 | 1.1 | 0.2 | 8.0 | 13.0 | 4.0 | 8.0 | 2.0 |
| GH17 | | 15.7 | 31.6 | 3.4 | 13.6 | 2.7 | 0.5 | 2.1 | 0.3 | 1.6 | 0.2 | 0.6 | 0.1 | 0.8 | 0.1 | 8.0 | 11.0 | 5.0 | 10.5 | 2.0 |
| GH34 | | 18.2 | 43.6 | 4.4 | 18.3 | 3.9 | 0.8 | 3.4 | 0.6 | 2.6 | 0.4 | 1.0 | 0.2 | 1.2 | 0.2 | 3.5 | 14.0 | 3.0 | 6.0 | 2.5 |
| GH35 | | 5.0 | 10.2 | 1.1 | 4.2 | 0.7 | 0.1 | 0.5 | 0.1 | 0.2 | 0.0 | 0.1 | 0.0 | 0.1 | 0.0 | 2.5 | 1.0 | 3.0 | 1.0 | 1.4 |
| GH38 | | 30.3 | 60.0 | 6.5 | 25.4 | 4.6 | 0.5 | 3.6 | 0.5 | 2.5 | 0.4 | 1.1 | 0.2 | 1.3 | 0.2 | 5.0 | 18.0 | 12.0 | 4.0 | 4.0 |
| GH39 | | 66.3 | 136.4 | 14.2 | 54.0 | 8.1 | 0.5 | 4.6 | 0.6 | 2.5 | 0.4 | 1.0 | 0.1 | 1.0 | 0.2 | 4.0 | 16.0 | 42.0 | 2.0 | 3.0 |
| GH61 | | 8.5 | 17.1 | 1.7 | 6.7 | 1.2 | 0.3 | 1.0 | 0.2 | 0.8 | 0.1 | 0.3 | 0.1 | 0.4 | 0.1 | 3.0 | 6.0 | 4.0 | 3.0 | 1.5 |
| AS69A | | 44.6 | 93.9 | 9.9 | 40.7 | 9.3 | 1.8 | 7.0 | 1.2 | 7.5 | 1.6 | 4.8 | 0.8 | 4.3 | 0.7 | 12.0 | 44.4 | 17.4 | 54.4 | 2.6 |
| GH23 | Pandukeshwar | 17.8 | 36.0 | 3.8 | 14.6 | 2.7 | 0.4 | 2.0 | 0.3 | 1.4 | 0.2 | 0.6 | 0.1 | 0.8 | 0.1 | 5.0 | 10.0 | 6.0 | 5.0 | 3.0 |
| GH26 | | 8.5 | 16.9 | 1.8 | 7.0 | 1.3 | 0.2 | 1.1 | 0.2 | 0.9 | 0.1 | 0.4 | 0.1 | 0.4 | 0.1 | 3.0 | 6.0 | 3.0 | 3.0 | 2.0 |
| GH27 | | 22.4 | 45.7 | 5.0 | 20.1 | 3.6 | 0.7 | 3.0 | 0.5 | 2.4 | 0.4 | 1.1 | 0.2 | 1.5 | 0.2 | 5.0 | 31.0 | 4.0 | 3.0 | 3.0 |
| GH47 | | 5.8 | 12.9 | 1.2 | 4.5 | 0.8 | 0.2 | 0.6 | 0.1 | 0.4 | 0.1 | 0.2 | 0.0 | 0.2 | 0.0 | 6.0 | 8.0 | 10.0 | 15.0 | 3.0 |
| GH47b | | 57.7 | 116.0 | 12.0 | 45.8 | 7.8 | 1.3 | 5.9 | 0.9 | 4.5 | 0.7 | 2.0 | 0.3 | 2.7 | 0.5 | 4.0 | 9.0 | 3.0 | 3.0 | 3.0 |
| AS27a2 | | 32.1 | 64.1 | 6.3 | 24.6 | 5.3 | 1.3 | 3.5 | 0.5 | 2.2 | 0.4 | 1.0 | 0.1 | 0.7 | 0.1 | 3.6 | 9.3 | 10.4 | 37.9 | 1.2 |
| AS27b | | 10.3 | 22.4 | 2.2 | 8.6 | 2.2 | 0.7 | 1.1 | 0.2 | 0.6 | 0.1 | 0.3 | 0.0 | 0.2 | 0.0 | 1.0 | 2.9 | 3.7 | 19.7 | 0.9 |
| AS28b | | 23.9 | 49.5 | 4.7 | 19.0 | 4.5 | 1.4 | 2.9 | 0.4 | 2.1 | 0.4 | 1.0 | 0.1 | 0.7 | 0.1 | 1.9 | 9.3 | 8.5 | 28.6 | 1.7 |
| AS29a | | 16.8 | 36.2 | 3.5 | 13.9 | 2.8 | 0.6 | 2.2 | 0.3 | 1.6 | 0.3 | 0.9 | 0.1 | 0.7 | 0.1 | 1.1 | 8.2 | 5.7 | 22.0 | 1.0 |
| AS30a | | 20.3 | 41.0 | 4.0 | 15.4 | 3.3 | 0.7 | 2.5 | 0.4 | 2.0 | 0.4 | 1.0 | 0.2 | 0.9 | 0.1 | 1.6 | 10.5 | 6.6 | 21.1 | 1.0 |
| AS31a | | 16.9 | 35.2 | 3.4 | 14.1 | 2.9 | 0.7 | 2.4 | 0.4 | 2.1 | 0.4 | 1.0 | 0.2 | 0.9 | 0.1 | 0.7 | 10.8 | 4.9 | 31.1 | 0.9 |
| AS32a | | 19.0 | 39.7 | 3.7 | 14.7 | 3.0 | 0.7 | 2.3 | 0.4 | 2.2 | 0.4 | 1.3 | 0.2 | 1.0 | 0.2 | 1.8 | 12.2 | 6.0 | 33.2 | 1.1 |
| AS33a | | 27.9 | 55.5 | 5.6 | 21.8 | 4.4 | 1.0 | 3.2 | 0.5 | 3.2 | 0.7 | 2.0 | 0.3 | 1.8 | 0.3 | 3.3 | 19.2 | 9.4 | 37.4 | 1.2 |
| AS34a | | 30.6 | 70.7 | 6.5 | 26.6 | 5.9 | 1.3 | 4.5 | 0.7 | 3.6 | 0.7 | 2.0 | 0.3 | 1.6 | 0.2 | 5.4 | 18.3 | 10.6 | 37.0 | 1.6 |
| AS50a | | 40.6 | 83.4 | 8.3 | 31.8 | 6.4 | 1.2 | 4.9 | 0.8 | 3.9 | 0.7 | 2.0 | 0.2 | 1.6 | 0.2 | 6.0 | 20.7 | 15.0 | 44.9 | 2.0 |
| AS54A | | 9.2 | 18.6 | 1.8 | 7.0 | 1.3 | 0.3 | 0.9 | 0.1 | 0.5 | 0.1 | 0.3 | 0.0 | 0.2 | 0.0 | | 2.8 | 1.6 | 22.3 | 0.4 |
| AS55A | | 18.2 | 38.4 | 3.7 | 14.6 | 3.0 | 0.7 | 2.4 | 0.4 | 2.1 | 0.4 | 1.1 | 0.2 | 0.9 | 0.1 | 1.1 | 11.6 | 5.4 | 19.8 | 1.4 |
| AS65A | | 35.6 | 75.8 | 7.2 | 27.6 | 6.3 | 1.6 | 4.2 | 0.6 | 2.9 | 0.4 | 1.1 | 0.1 | 0.6 | 0.1 | 2.9 | 11.0 | 11.7 | 33.0 | 1.6 |
| AS70A | | 16.3 | 33.7 | 3.3 | 12.1 | 2.6 | 0.6 | 1.8 | 0.3 | 1.6 | 0.3 | 0.9 | 0.1 | 0.7 | 0.1 | 0.8 | 8.6 | 3.9 | 22.4 | 0.7 |
| AS71B | | 29.5 | 59.8 | 5.8 | 21.5 | 4.8 | 1.2 | 3.2 | 0.5 | 2.2 | 0.4 | 1.2 | 0.2 | 1.0 | 0.2 | 5.0 | 11.2 | 9.4 | 49.7 | 1.3 |
| AS72B | | 48.6 | 99.6 | 10.4 | 47.0 | 11.6 | 3.1 | 11.3 | 2.0 | 11.4 | 2.3 | 6.5 | 1.0 | 5.6 | 0.8 | 6.8 | 75.8 | 11.8 | 54.1 | 5.2 |
| AS74a | | 12.3 | 27.1 | 2.5 | 10.0 | 2.1 | 0.5 | 1.7 | 0.3 | 1.4 | 0.3 | 0.7 | 0.1 | 0.6 | 0.1 | 0.1 | 7.3 | 3.4 | 10.7 | 1.0 |
| AS75A | | 13.6 | 29.5 | 2.7 | 11.0 | 2.5 | 0.6 | 1.8 | 0.3 | 1.6 | 0.3 | 0.8 | 0.1 | 0.6 | 0.1 | 0.3 | 8.1 | 3.8 | 14.9 | 0.7 |
| AS76A | | 13.5 | 27.2 | 2.6 | 10.4 | 2.4 | 0.7 | 1.6 | 0.2 | 1.2 | 0.2 | 0.6 | 0.1 | 0.5 | 0.1 | 1.5 | 5.9 | 4.2 | 22.8 | 0.6 |
| AS76C | | 15.4 | 32.1 | 3.1 | 12.2 | 2.6 | 0.6 | 1.9 | 0.3 | 1.5 | 0.3 | 0.7 | 0.1 | 0.6 | 0.1 | 1.1 | 7.4 | 5.9 | 19.4 | 0.8 |
| AS77A | | 13.7 | 28.8 | 2.8 | 11.1 | 2.3 | 0.5 | 1.8 | 0.3 | 1.6 | 0.3 | 0.7 | 0.1 | 0.5 | 0.1 | 0.3 | 7.5 | 3.8 | 14.3 | 0.7 |
| AS78A | | 14.7 | 28.5 | 2.8 | 10.8 | 3.0 | 1.1 | 1.6 | 0.2 | 1.2 | 0.2 | 0.6 | 0.1 | 0.5 | 0.1 | 1.6 | 6.1 | 4.6 | 24.3 | 0.6 |
| AS79A | | 14.5 | 30.3 | 3.0 | 11.8 | 2.6 | 0.6 | 1.9 | 0.3 | 1.5 | 0.3 | 0.8 | 0.1 | 0.6 | 0.1 | 1.0 | 7.9 | 4.9 | 20.2 | 0.7 |
| AS79b | | 17.3 | 35.0 | 3.3 | 12.9 | 2.9 | 0.8 | 1.7 | 0.3 | 1.5 | 0.3 | 0.8 | 0.1 | 0.6 | 0.1 | 1.0 | 8.5 | 4.9 | 19.9 | 0.9 |
| AS80b | | 10.2 | 22.1 | 2.0 | 8.5 | 1.9 | 0.4 | 1.4 | 0.2 | 1.2 | 0.2 | 0.6 | 0.1 | 0.5 | 0.1 | | 6.2 | 3.4 | 15.1 | 1.0 |
| AS81A | | 31.0 | 61.3 | 6.1 | 24.8 | 5.1 | 1.3 | 4.2 | 0.7 | 3.6 | 0.7 | 2.0 | 0.3 | 1.5 | 0.2 | 2.5 | 19.9 | 12.4 | 29.2 | 1.7 |
| AS81B | | 17.3 | 35.1 | 3.4 | 13.4 | 2.7 | 0.6 | 2.0 | 0.3 | 1.8 | 0.4 | 1.1 | 0.2 | 1.0 | 0.2 | 1.7 | 10.5 | 5.1 | 33.1 | 1.0 |
| AS83A | | 16.2 | 33.6 | 3.3 | 12.7 | 3.2 | 0.8 | 1.8 | 0.3 | 1.5 | 0.3 | 0.7 | 0.1 | 0.5 | 0.1 | 0.7 | 7.4 | 4.6 | 18.6 | 0.8 |
| AS84A | | 21.0 | 43.3 | 4.1 | 16.2 | 3.3 | 0.7 | 2.5 | 0.4 | 1.9 | 0.3 | 0.8 | 0.1 | 0.5 | 0.1 | 0.5 | 9.0 | 6.5 | 18.5 | 1.2 |
| AS85A | | 19.0 | 41.3 | 3.8 | 14.7 | 3.8 | 1.0 | 2.3 | 0.4 | 2.0 | 0.3 | 0.9 | 0.1 | 0.9 | 0.1 | 0.9 | 9.0 | 5.7 | 17.9 | 0.9 |
| GH29 | Badrinath | 6.1 | 12.3 | 1.3 | 4.8 | 0.9 | 0.2 | 0.7 | 0.1 | 0.4 | 0.1 | 0.2 | 0.0 | 0.2 | 0.0 | 3.0 | 2.5 | 2.0 | 2.0 | 1.4 |
| GH31 | | 12.2 | 25.2 | 2.7 | 10.7 | 2.1 | 0.4 | 1.7 | 0.2 | 1.0 | 0.1 | 0.3 | 0.0 | 0.3 | 0.1 | 8.0 | 5.0 | 4.0 | 7.0 | 3.0 |
| GH32 | | 4.6 | 9.9 | 1.1 | 3.8 | 1.0 | 0.2 | 0.9 | 0.2 | 1.2 | 0.2 | 0.6 | 0.1 | 0.8 | 0.1 | 4.0 | 10.0 | 6.8 | 2.0 | 3.0 |
| GH33 | | 21.8 | 45.7 | 4.9 | 18.8 | 4.1 | 0.7 | 3.2 | 0.5 | 1.7 | 0.2 | 0.4 | 0.0 | 0.3 | 0.0 | 4.0 | 8.0 | 9.0 | 3.0 | 4.0 |
| GH33b | | 52.4 | 103.4 | 10.6 | 41.4 | 6.9 | 1.0 | 5.3 | 0.8 | 3.7 | 0.6 | 1.5 | 0.2 | 1.6 | 0.2 | 3.0 | 15.0 | 3.5 | 5.0 | 3.0 |
| GH54 | | 2.9 | 6.0 | 0.6 | 2.3 | 0.5 | 0.1 | 0.4 | 0.1 | 0.3 | 0.1 | 0.1 | 0.0 | 0.2 | 0.0 | 7.0 | 10.0 | 2.5 | 5.0 | 1.0 |

Arabian/Nubian shield (Harms et al., 1990; Windley et al., 1996). An Antarctic or Arabian source is substantiated by detrital zircon ages from Saudi Arabia (Agar et al., 1992), Israel (Avigad et al., 2003), Jordan (Kolodner et al., 2006), Ethiopia (Avigad et al., 2007), and Antarctica (Goodge et al., 2004) which show similar peaks as the Greater Himalayan Sequence (DeCelles et al., 2000; Upreti and Yoshida, 2005; Yoshida and Upreti, 2006).

## 6. Depositional models

Current models for the origin of the Greater Himalayan Sequence include a single passive margin (Frank et al., 1973; Colchen et al., 1982), Carboniferous, intra-cratonic extension (Yin, 2006), and an active continental margin (DeCelles et al., 2000; Gehrels et al., 2003, 2006; Yin et al., 2010a,b). The single passive margin model states that the Lesser Himalaya Sequence, the Greater Himalayan Sequence, and the Tethyan Himalayan Sequence were deposited on the same north-facing continental margin of northern India. The three sequence represent increasingly off-shore facies from the shelf to slope. Jamieson et al. (2006) claimed that numerical models of channel flow also predict a single passive margin model with a more distal Indian source for the Greater Himalayan Sequence. However, this hypothesis is contrary to both stratigraphic, isotopic, and geochemical evidence (Ahmad et al., 2000; DeCelles et al., 2000; Robinson et al., 2001; Yoshida and Upreti, 2006; Imayama and Arita, 2007; Murphy, 2007). The Lesser Himalayan Sequence has an isotopic and detrital zircon signature of the Indian Shield with more negative epsilon Nd values than the Greater Himalayan Sequence and Tethyan Himalayan Sequence which have more juvenile epsilon Nd values and a detrital zircon signature more akin to eastern Antarctica and the Arabian Shield (Ahmad et al., 2000; Imayama and Arita, 2007; DeCelles et al., 2000; Yoshida and Upreti, 2006).

The Carboniferous-extension model (Yin, 2006) claims that the Lesser Himalayan Sequence and the Greater Himalayan Sequence strata were juxtaposed by a Carboniferous north-dipping normal fault system prior to Cenozoic deformation. This model is based upon the lack of Ordovician to Carboniferous strata in the Lesser

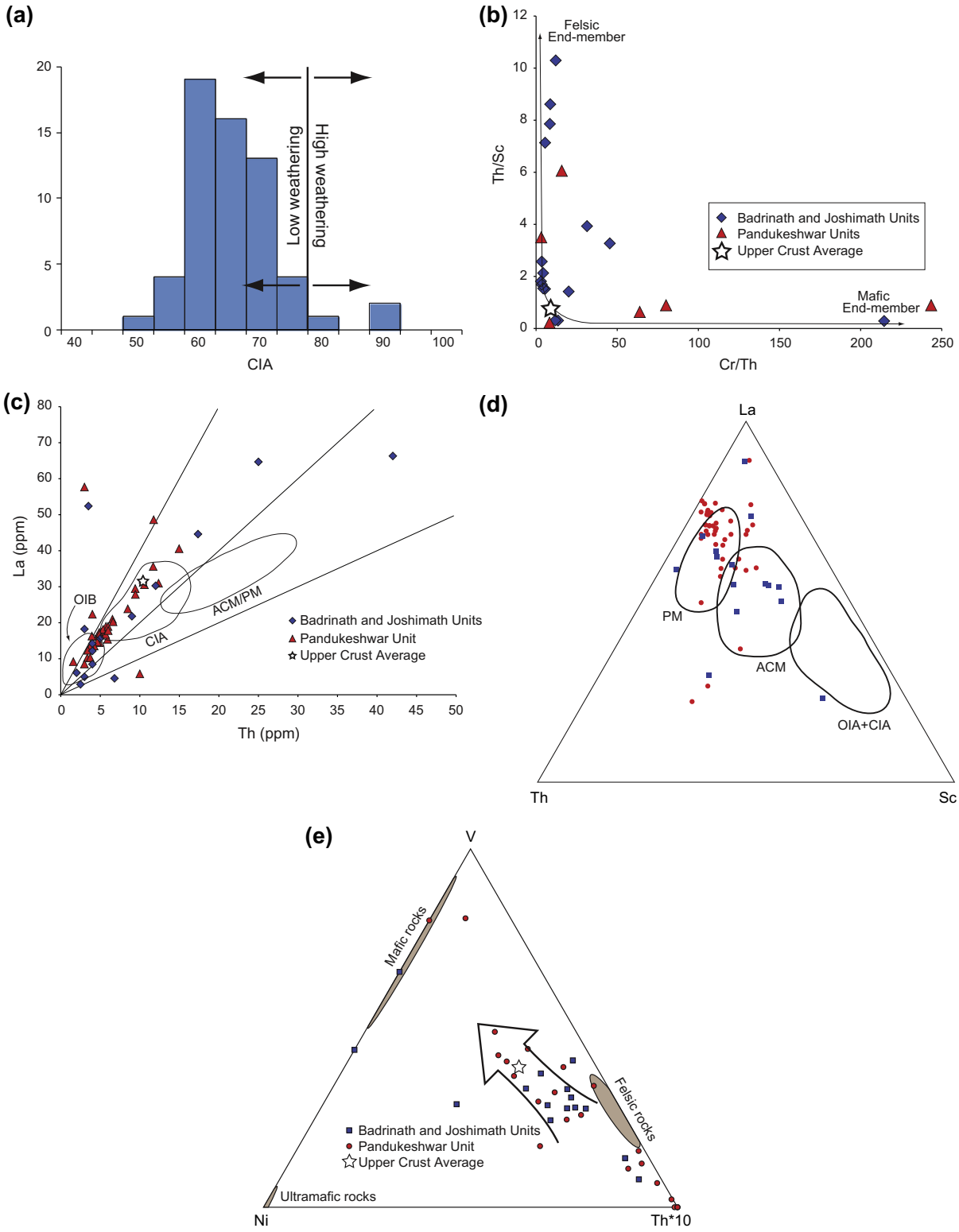


**Fig. 3.** Discrimination diagrams with trace elements of the Garhwal Greater Himalayan samples. (a) Histogram of CIA ($Al_2O_3/[Al_2O_3 + CaO + Na_2O + K_2O] \times 100$) (Nesbitt and Young, 1982). Values higher than 75 indicate high degrees of weathering (Long et al., 2008). (b) Cr/Th vs Th/Sc. (c) Plot of La vs Th displaying provenance fields after Bhatia (1983). (d) La–Th–Sc diagram plotting provenance fields after Bhatia and Crook (1986). OIA: island arc, CIA: continental arc, ACM: active continental margin, PM: passive margin. (e) V–Ni–Th * 10 diagram plotting composition fields of felsic, mafic, and ultramafic rocks after Bracciali et al. (2007). Average upper crust composition after Rudnick (2005). The bulk of the samples lie near the average upper crust composition (PLUC) with a mixing trend towards the average mafic composition. This mixing trend is possibly due a mafic component in the detritus of the Greater Himalayan Sequence. Circle and square symbols are samples from psammitic and pelitic units respectively.

Himalayan Sequence. This model, however, assumes the source of the Greater Himalayan Sequence and Tethyan Himalayan Sequence is the northern Indian margin which is also contrary to isotopic, and geochemical evidence.

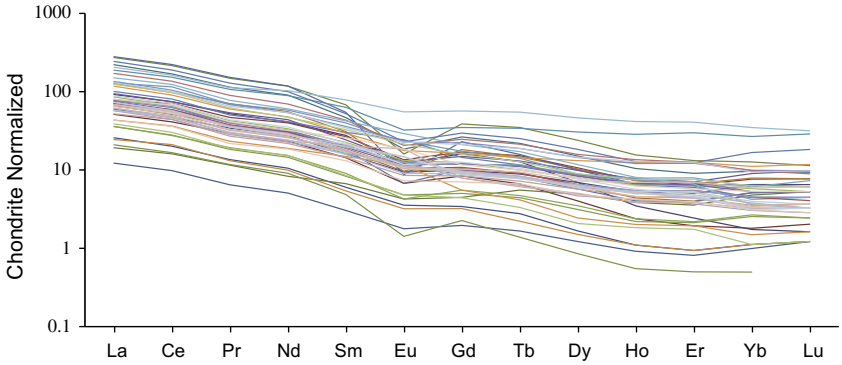


**Fig. 4.** Chondrite-normalized REE patterns for the formations of the Greater Himalayan Sequence. Normalization factors from McDonough and Sun (1995).

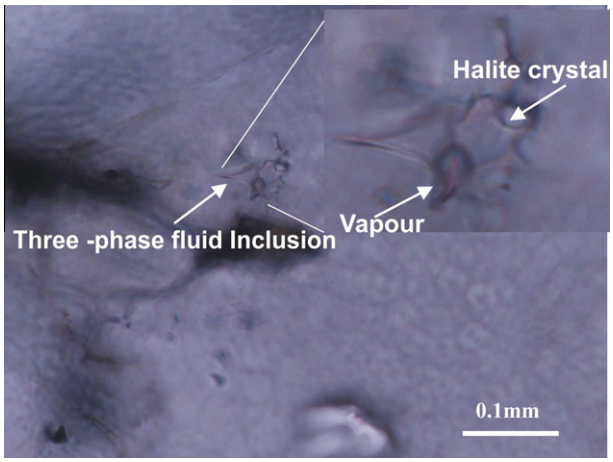


**Fig. 5.** Photomicrograph of characteristic fluid inclusion from the Pandukeshwar formation.

**Table 2**
Homogenization temperatures of three-phase fluid inclusions from the Pandukeshwar formation.

| Sample | *T* (C°) |
|---|---|
| FL1 | 225 |
| FL2 | 225 |
| FL3 | 226 |
| FL4 | 228 |
| FL5 | 229 |
| FL6 | 231 |
| FL7 | 232 |
| FL8 | 233 |
| FL9 | 234 |
| FL10 | 234 |
| FL11 | 235 |
| FL12 | 235 |
| FL13 | 236 |
| FL14 | 237 |
| FL15 | 238 |

The data presented here matches best with the active continental margin model (DeCelles et al., 2000; Gehrels et al., 2003, 2006; Yin et al., 2010a,b). The sediments derived from this active continental margin is thought to have been derived from the East African Orogeny (DeCelles et al., 2000; Gehrels et al., 2003, 2006) and/or the East Antarctic Orogeny (Yoshida and Upreti, 2006) or the more proximal Bhimphedian Orogeny of Northern India (Garzanti et al., 1986; Cawood et al., 2007).

The lack of deformation associated with the accretion of the Greater Himalayan Sequence to the northern Indian margin requires that either the collision involved a significant amount of oblique motion, the deformed portion was subducted beneath Asia during the Cenozoic collision, or that last stage post accretion deposition buried the deformation.

Several potential tectonic events have been proposed as the source for the Greater Himalayan Sequence. In light of this new data, each potential tectonic event will be investigated to identify the most likely to have sourced the sediment of the Greater Himalayan Sequence.

## 7. East African Orogeny

The East African Orogeny extends from the southern tip of Africa to northern Arabia and took place from >620 to 530 Ma (Katz et al., 2004). Garfunkel (1999), identified three tectonic stages in the northernmost East African Orogeny: orogenic (>600 Ma), transitional (600–530 Ma), and platform (<530 Ma). The youngest post-tectonic intrusions in northern portion of the orogeny are 613–606 Ma (Miller et al., 2003). Because the Greater Himalayan Sequence contains detrital zircons younger than 600 Ma, the East African Orogeny alone cannot be responsible for the deposition of the Greater Himalayan Sequence.

## 8. East Antarctic Orogeny

The late Mesoproterozoic East Antarctic orogeny occurred along East Antarctica. This orogen took place along the eastern margin of India, and into the western and southwestern margins of Australia (Yoshida, 1995; Yoshida et al., 2003; Yoshida and Upreti, 2006) during the latest Neoproterozoic–early Palaeozoic times. Age distribution peaks of zircons from these areas are mostly composed of ca. 900–1300 Ma and ca. 500–600 Ma. While the East Antarctic Orogeny provides a potential source region for the detrital zircons found in the Greater Himalayan Sequence, it does not account for the deformed Cambrian-age strata found in the western Himalaya (Wiesmayr and Grasemann, 2002).

## 9. Bhimphedian Orogeny

In the Kathmandu region transgressive Ordovician strata lie along an angular unconformably on older successions and are widespread along the Indian part of Gondwana (Pogue et al., 1999; Cawood et al., 2007). Wiesmayr et al. (1998) and Pogue et al. (1999) document uplift and mesoscopic folding of early Cambrian strata cut be an Ordovician unconformity. Baig et al. (1988) also provide evidence for an angular disconformity between undeformed Lower Cambrian rocks and gently folded, weakly metamor-

phosed Precambrian rocks west of the western syntaxis and outside the majority of Cenozoic Himalayan deformation. The presence of Ordovician conglomerate on an angular unconformity are interpreted to have accumulated in the foreland basin of a thrust belt that was active during Late Cambrian(?) through Middle Ordovician time (Garzanti et al., 1986). The apparent cessation of Cambrian sedimentation of what is now the Lesser Himalayan Sequence during early Paleozoic time may also record the onset of early Paleozoic tectonism (Brookfield, 1993; Valdiya, 1995). Gehrels et al. (2006) also noted that 520–500 Ma detrital zircon grains analyzed from arkosic sediments in the Kathmandu region could reflect further input from this arc system. Myrow et al. (2006, 2009) reported Cambrian-age passive margin sedimentation in the Spiti and Zanskar valleys and claimed that this precludes the presence of an arc system at this time. These strata are however, unconstrained using geochronologic techniques. Furthermore, Cawood et al. (2007) describe a sequence of events where a passive margin preceded and followed the Bhimphedian Orogeny. Therefore, the Cambrian sequences studied in Myrow et al. (2006, 2009) could potentially represent strata deposited before and after the Bhimphedian Orogeny. These rocks are separated by a sharp break from non-marine arenites and conglomerates of mid-Ordovician age (Cawood et al., 2007).

In comparing these three orogenic events, it appears that the Bhimphedian Orogeny is the most likely source for the sediments in the Greater Himalayan Sequence.

## 10. Sequence of depositional and tectonic events

### *10.1. Early Proterozoic–Late Proterozoic (<1600–800 Ma)*

During early Proterozoic the Lesser Himalayan Sequence was deposited off the northern margin of India sourced along a passive margin with sediments shed from the interior of the Indian Craton (Yoshida and Upreti, 2006; Imayama and Arita, 2007) and/or along a continental arc setting from 1780 to 1880 Ma (Kohn et al., 2010) (see Fig. 6a). Célérier et al. (2009) extended the age of deposition of the Lesser Himalayan Sequence in the Garhwal/Kumaun regions of India between 1880 and 800 Ma.

### *10.2. Late Proterozoic–Early Paleozoic (~820–480 Ma)*

DeCelles et al. (2000) bracketed the age of deposition of the Greater Himalayan Sequence in Central Nepal from ~820 to 480 Ma from detrital zircon and cross cutting granite U–Pb ages, with a significant zircon population between 520 and 480 Ma. Parrish and Hodges (1996) also found that the presence of 1000–800 Ma detrital zircons in the Greater Himalayan Sequence demonstrate that the sedimentary precursors of these rocks cannot be older than Neoproterozoic. During this time, India was bordered by Africa/Arabia to the west, Antarctica to the east, and the Paleo-Tethys Ocean to the North (Scotese, 1997) (Fig. 6b). Following the earliest deposition of the Greater Himalayan Sequence, an igneous/contractional event ca. 520–480 Ma (the Bhimphedian Orogeny after Cawood et al., 2007) took place along the entire southern margin of India and the Greater Himalayan Sequence terrain (Cawood et al., 2007; Yin et al., 2010a,b) (Fig. 6c). This event correlates with the emplacement ages of the Lesser Himalayan Igneous Belt which is a group of syncollisional granitoids found along the entire length of the Himalayan Range in between the Lesser and Greater Himalayan Sequences (Fig. 6d).

According to Cawood et al. (2007), the Bhimphedian Orogeny is an Andean-type orogenic event that was active ca. 530–480 Ma. The magmatic arc was associated with felsic, andesitic and basaltic volcanism which overlaps and succeeded by regional deformation, accretion of the Greater Himalayan Sequence/Terrane, crustal melting and S-type granite emplacement that extended to 470 Ma (Cawood et al., 2007). The volcanic rocks of Cambrian-age that occur in the western Tethyan Himalaya (Garzanti et al., 1986; Valdiya, 1995) could be a potential source region for the Greater Himalayan Sequence. Garzanti et al. (1986) showed that the volcanics include low-K tholeiites with trace elements indicative of an immature arc environment. Yin et al. (2010a) also recognize the presence of a Cambrian-age arc and claim that the Eastern Ghats-Shillong Arc (or the East Antarctic orogeny) is the eastward continuation of the Paleo-Hima Arc (or the Bhimphedian Orogeny). They also claim that in Bhutan, the Greater Himalayan Sequence may be a tectonic mixture of Indian crystalline basement, its Proterozoic–Cambrian cover sequence and an early Paleozoic arc.

Even though the East African and East Antarctic orogeny are potential source regions for the Greater Himalayan Sequence, the Bhimphedian Orogeny provides a more proximal and therefore a more plausible source. Evidence for the early Paleozoic Bhimphedian Orogeny and magmatic activity is widespread in the western Himalaya (e.g. Garzanti, 1993; Garzanti, 1999; Argles et al., 2003; Gehrels et al., 2003, 2006). During this deformation, metamorphism, plutonism, uplift, and erosion developed within a south-vergent thrust belt that was active during Late Cambrian(?) – Middle Ordovician time (Gehrels et al., 2006). Whether the nature of this accretion took place as an orthogonal collision or an oblique collision it is unclear and the lack of extensive Cambro-Ordovician-age shortening precludes the possibility of a significant orthogonal collision.

The origin of the ~500 Ma granites has also been related to both crustal extension (Debon et al., 1986; LeFort et al., 1983; Le Fort et al., 1986; Girard and Bussy, 1999; Miller et al., 2001) and orogenic tectonism (Gehrels et al., 2003, 2006). The possibility of a widespread extensional event cannot be discounted as the tectonic setting for the sediments some of the Greater Himalayan Sequence, however an extensional model alone cannot account for the active margin geochemical signature and isotopic compositions distinct from the sediments shed from the passive margin of India (Parrish and Hodges, 1996; Ahmad et al., 2000; Imayama and Arita, 2007).

### *10.3. Early Paleozoic–Late Paleozoic (480–150 Ma)*

Following the accretion of the Greater Himalayan Sequence and formation of the Lesser Himalayan Igneous Belt during Late Cambrian to Early Ordovician time, the widespread inundation of the Tethys Ocean deposited the Tethyan Himalayan Sequence nonconformably over the Lesser Himalayan Sequence and Greater Himalayan Sequence (Brookfield, 1993; Pogue et al., 1999). Inundation of the Tethys Ocean was accommodated by the Permian-age rifting of the Lhasa terrane in the northern Himalaya (Yin and Harrison, 2000; Yin et al., 2010a). This suggests that the rifting occurred to the north of the previously accreted Greater Himalayan Sequence. The deposition of the Tethyan Himalayan Sequence continued throughout the remainder of Paleozoic time (Pogue et al., 1999) and this newly formed passive margin continued to develop continuously until the latest Cretaceous when the collision between India and Asia began affecting its sedimentary facies pattern and its rate of subsidence (Shi et al., 1996; Willems et al., 1996). This deposition took place both from the Indian craton to the South as well as from the Lhasa terrane to the North evidenced by detrital zircons from both affinities (DeCelles et al., 2000).

## 11. Conclusions

The depositional setting of the Greater Himalayan Sequence has previously identified as the passive margin along the northern edge of India; however, geochemical evidence from this study and previous detrital zircon studies do not support this hypothesis. A

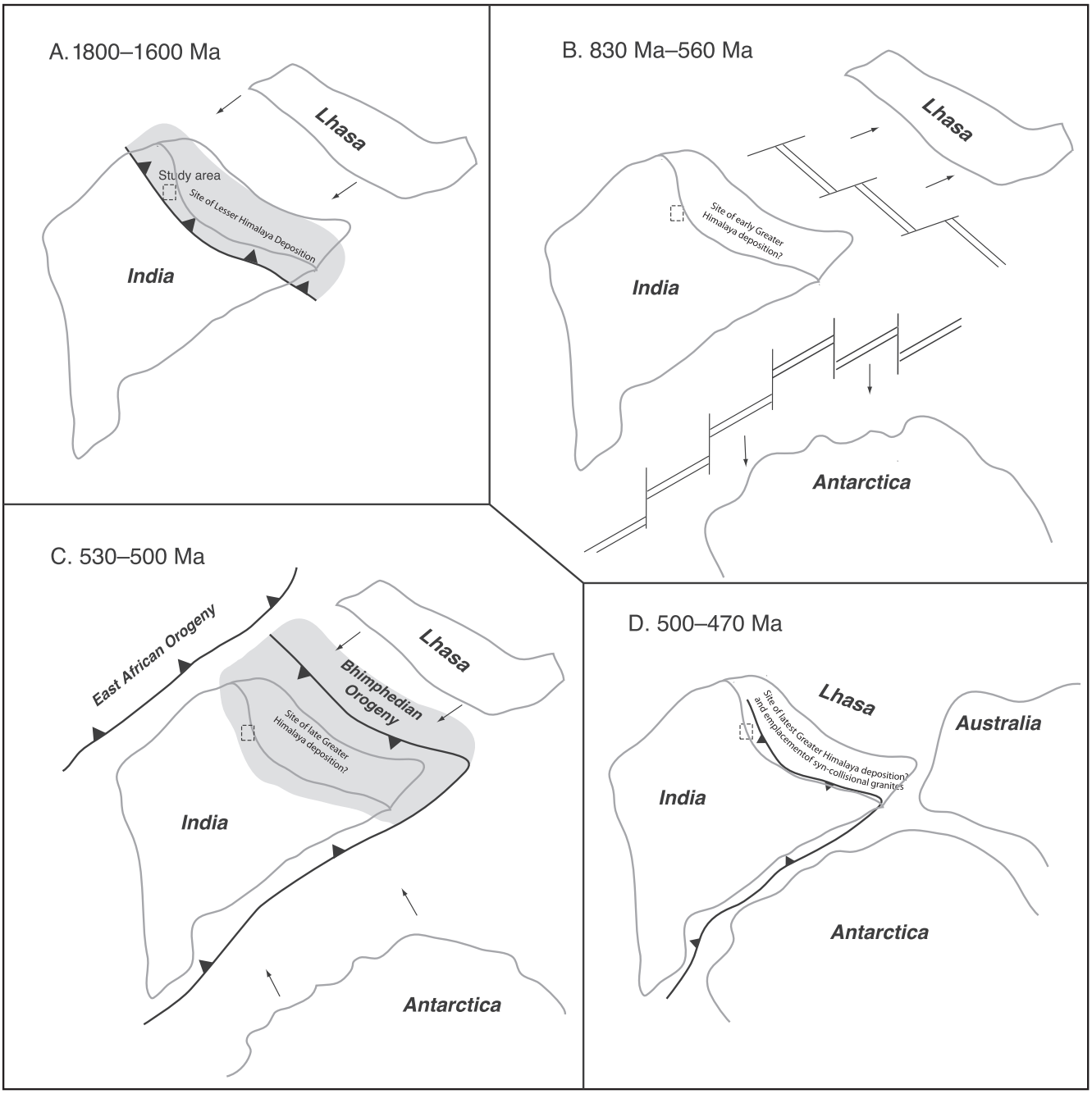


**Fig. 6.** Tectonic evolution of India/Gondwana during the formation of the major lithotectonic unit of the Himalaya (modified after Kohn et al., 2010 and Yin et al., 2010a). (A) 1800–1600 Ma: deposition of the Lesser Himalayan Sequence along a continental volcanic arc; (B) 830–560 Ma: separation of Lhasa and Antarctica and development of a passive continental margin along the east side of India; (C) 530–500 Ma: subduction along the east and north sides of India and the development of the Bhimphedian and East African and East Antarctic orogeny; (D) 500–470 Ma: collision of India and Antarctica along the Eastern Ghats orogen and collision between India and Lhasa along the Bhemphedian orogeny.

more plausible hypothesis while taking these data into consideration is an active continental margin. This hypothesis supports other evidence for the Bhimphedian Orogeny that was active from 530 to 490 Ma. Following the deposition of the Greater Himalayan Sequence along this active continental margin, the sequence was tectonically consolidated with the northern margin of India placing it structurally above the Lesser Himalayan Sequence. After this early Paleozoic orogeny, the northern margin of India was covered by passive margin sediments that accumulated in the Paleo-tethys Ocean until the late Paleozoic breakup of northern India and the migration of crustal fragments from India to central Asia.

## Acknowledgements

We would like to thank the Wadia Institute of Himalayan Geology and Dave Tingy of the Brigham Young University, Geological Sciences Department for assistance in the geochemical analysis. We are also grateful to Michael J. Dorais for his constructive discussions and comments.

## References

Agar, R.A., Stacey, J.S., Whitehouse, M.J., 1992. Archaean to Late-Proterozoic Evolution of the Southern Afif Terrane, Kingdom of Saudi Arabia: A Study

Using Sm–Nd and Ion-probe U–Pb Zircon Geochronology. Saudi Arabian Directorate General of Mines and Geology OF-10-15.
Ague, J.J., 2003. Fluid infiltration and transport of major, minor, and trace elements during regional metamorphism of carbonate rocks, Wepawaug Schist, Connecticut, USA. American Journal of Science 303, 753–816.
Ahmad, T., Harris, N., Bickle, M., Chapman, H., Bunbury, J., Prince, C., 2000. Isotopic constraints on the structural relationships between the Lesser Himalayan Series and the High Himalayan Crystalline Series, Garhwal Himalaya. Geological Society of America Bulletin 112, 467–477.
Al-Juboury, A.I., Ghazal, M.M., McCain, T.M., 2009. Detrital chromian spinels from Miocene and Holocene sediments of northern Iraq: provenance implications. Journal of Geosciences 54, 289–300.
Argles, T., Foster, G., Whittington, A., Harris, N., George, M., 2003. Isotope studies reveal a complete Himalayan section in the Nanga Parbat syntaxis. Geology 31, 1109–1112.
Avigad, D., Kolodner, K., McWilliams, M., Persing, H., Weissbrod, T., 2003. Origin of northern Gondwana Cambrian sandstone revealed by detrital zircon SHRIMP dating. Geology 31, 227–230.
Avigad, D., Stern, R.J., Beyth, M., Miller, N., McWilliams, M.O., 2007. Detrital zircon U–Pb geochronology of Cryogenian diamictites and Lower Paleozoic sandstone in Ethiopia (Tigrai) Age constraints on Neoproterozoic glaciation and crustal evolution of the southern Arabian–Nubian Shield. Precambrian Research 154, 88–106.
Baig, M.S., Lawrence, R.D., Snee, L.W., 1988. Evidence for late Precambrian to early Cambrian orogeny in northwest Himalaya, Pakistan. Geological Magazine 125, 83–86.
Bhatia, M.R., 1983. Plate tectonics and geochemical composition of sandstones. Journal of Geology 91, 611–627.
Bhatia, M.R., Crook, K.A.W., 1986. Trace element characteristics of greywackes and tectonic setting discrimination of sedimentary basins. Contributions of Mineralogy and Petrology 92, 181–193.
Bracciali, L., Marroni, M., Pandolfi, L., Rocchi, S., 2007. Geochemistry and petrography of Western Tethys Cretaceous sedimentary covers (Corsica and Northern Apennines): from source areas to configuration of margins. Geological Society of America Special Paper 420.
Brookfield, M.E., 1993. The Himalayan passive margin from Precambrian to Cretaceous times. Sedimentary Geology 4, 1–35.
Camiré, G.E., Laflèche, M.R., Ludden, J.N., 1993. Archaean metasedimentary rocks from the northwestern Pontiac Subprovince of the Canadian Shield: chemical characterization, weathering and modeling of the source areas. Precambrian Research 62, 285–305.
Cathelineau, M., Dubessy, J., Marignac, C., Poty, B., Weisbrod, A., 1988. Fluids in granitic environment. Rendiconti della Societa Italiana di Mineralogia é Petrologia 43, 263–274.
Cawood, P.A., Johnson, M.R.W., Nemchin, A.A., 2007. Early Palaeozoic orogenesis along the Indian margin of Gondwana: tectonic response to Gondwana assembly. Earth and Planetary Science Letters 255, 70–84.
Célérier, J., Harrison, T.M., Webb, A.A.G., Yin, A., 2009. The Kumaun and Garwhal Lesser Himalaya, India. Part 1, Structure and stratigraphy. Geological Society of America Bulletin 121, 1262–1280.
Colchen, M., Bassoullet, J.P., Mascle, G., 1982. La paleogeographie des orogenes, l'example de l'Himalaya. Memoir Geologie l'Université de Dijon 7, 453–471.
Cullers, R.L., Bock, B., Guidotti, C., 1997. Elemental distributions and neodymium isotopic compositions of Silurianmetasediments, western Maine, USA: redistribution of the rare earth elements. Geochimica Cosmochimica Acta 61, 1847–1861.
Dasgupta, S., Chakraborty, S., Neogi, S., 2009. Petrology of an inverted Barrovian sequence of Metapelites in Sikkim Himalaya, India: constraints on the tectonics of inversion. American Journal of Science 309, 43–84.
Debon, F., Lefort, P., Sheppard, S.M.F., Sonet, J., 1986. The four plutonic belts of the TransHimalaya–Himalaya: a chemical, mineralogical, isotopic, and chronological synthesis along a Tibet–Nepal section. Journal of Petrology 27, 219–250.
DeCelles, P.G., Gehrels, G.E., Quade, J., LaReau, B., Spurlin, M., 2000. Tectonic implications of U–Pb zircon ages of the Himalayan orogenic belt in Nepal. Science 288, 497–499.
De Vivo, B., Ayuso, R.A., Belkin, H.E., Lima, A., Messina, A., Viscardi, A., 1991. Rock chemistry and fluid inclusion studies as exploration tools for ore deposits in the Sila batholith, southern Italy. Journal of Geochemical Exploration 40, 291–310.
Frank, W., Hoinkes, G., Miller, C., Purtscheller Richter, W., Thoni, M., 1973. Relations between metamorphism and orogeny in a typical section of the Indian Himalayas. Tschermaks Mineralogische und Petrographische Mitteilungen 20, 303–332.
Gairola, V.K., Srivastava, H.B., 1987. Deformational and metamorphic studies in the central crystallines around Joshimath District Chamoli, UP. In: Proceedings of the National Seminar on Tertiary Orogeny in Indian Subcontinent, pp. 49–63.
Gao, S., Wedepohl, K.H., 1995. The negative Eu anomaly in Archean sedimentary rocks: implications for decomposition, age and importance of their granitic source. Earth and Planetary Science Letters 133, 81–94.
Garfunkel, Z., 1999. History and paleogeography during the Pan-African orogen to stable platform transition Reappraisal of the evidence from the Elat area and the Arabian–Nubian Shield. Israel Journal of Earth Sciences 48, 135–157.
Garzanti, E., 1993. Sedimentary evolution and drowning of a passive margin shelf (Giumal Group; Zanskar Tethys Himalaya, India): palaeoenvironmental changes during final break-up of the Gondwanaland. In: Treloar, P.J., Searle, P.M. (Eds.), Himalayan Tectonics, The Geological Society Special Publication, 74, 277–298.
Garzanti, E., 1999. Stratigraphy and sedimentary history of the Nepal Tethys Himalaya passive margin. Journal of Asian Earth Sciences 17, 805–827.
Garzanti, E., Casnedi, R., Jadoul, F., 1986. Sedimentary evidence of a Cambro-Ordovician orogenic event in the northwestern Himalaya. Sedimentary Geology 48, 237–265.
Gehrels, G.E., DeCelles, P.G., Martin, A., Ojha, T.P., Pinhassi, G., Upreti, B.N., 2003. Initiation of the Himalayan orogen as an early Paleozoic thin-skinned thrust belt. GSA Today 13, 4–9.
Gehrels, G.E., DeCelles, P.G., Ojha, T.P., Upreti, B.N., 2006. Geologic and geochronologic evidence for early Paleozoic tectonism in the Kathmandu thrust sheet, central Nepal Himalaya. Geological Society of America Bulletin 118, 185–198.
Girard, M., Bussy, F., 1999. Late Pan-African magmatism in the Himalaya: new geochronological and geochemical data from the Ordovician Tso Morari Metagranites (Ladakh, NW India). Schweizer Mineralogische und Petrographische Mitteilungen 79, 399–417.
Goodge, J.W., Williams, I.S., Myrow, P., 2004. Provenance of Neoproterozoic and lower Paleozoic siliciclastic rocks of the central Ross orogen, Antarctica: detrital record of rift-, passive-, and active-margin sedimentation. GSA Bulletin 116, 1253–1279.
Gururajan, Choudhuri, 1999. Ductile thrusting metamorphism and normal faulting in Dhauliganga Valley, Garhwal Himalaya. Himalayan Geology 20, 19–29.
Harms, U., Schandelmeier, H., Darbyshire, D.P.F., 1990. Pan-African reworked early/middle Proterozoic crust in NE Africa west of the Nile: Sr and Nd isotope evidence. Journal of the Geological Society of London 147, 859–872.
Hofmann, A., 2005. The geochemistry of sedimentary rocks from the Fig Tree Group, Barberton greenstone belt: implications for tectonic, hydrothermal and surface processes during mid-Archaean times. Precambrian Research 143, 23–49.
Imayama, Arita, 2007. Nd isotopic data reveal the material and tectonic nature of the Vaikrita thrust zone in Nepal Himalaya. Tectonophysics 451, 265–281.
Jamieson, R.A., Beaumont, C., Nguyen, M.H., Grujic, D., 2006. Provenance of the Greater Himalayan Sequence and associated rocks: predictions of channel flow models. Geological Society, London Special Publications 2006, pp.165–182.
Katz, O., Beyth, M., Miller, N., Stern, R., Avigad, D., Basu, A., Anbar, A., 2004. A late Neoproterozoic (<630 Ma) high-magnesium andesite suite from southern Israel: implications for the consolidation of Gondwanaland. Earth and Planetary Science Letters 218, 475–490.
Kohn, M.J., Paul, S.K., Corrie, S.L., 2010. The lower Lesser Himalayan sequence: a Paleoproterozoic arc on the northern margin of the Indian plate. GSA Bulletin 122, 323–335.
Kolodner, K., Avigad, D., McWilliams, M., Wooden, J.L., Weissbrod, T., Feinstein, S., 2006. Provenance of north Gondwana Cambrian–Ordovician sandstone: U–Pb SHRIMP dating of detrital zircons from Israel and Jordan. Geological Magazine 143, 367–391.
LeFort, P., Debon, F., Sonet, J., 1983. The Lower Paleozoic "Lesser Himalayan" granitic belt: Emphasis on the Simchar pluton of central Nepal. In: Shams, F.A. (Ed.), Granites of the Himalayas, Karakorum, and Hindu Kush. Punjab University, Lahore, pp. 235–255.
Le Fort, P., Debon, F., Pecher, A., Vidal, P., 1986. The 500 Ma magmatic event in the Alpine of southern Asia: a thermal episode at Gondwana scale. Science Terra 47, 191–209.
Li, Q., Liu, S., Han, B., Zhang, J., Chu, Z., 2005. Geochemistry of metasedimentary rocks of the Proterozoic Xingxingxia complex: implications for provenance and tectonic setting of the eastern segment of the Central Tianshan Tectonic Zone, northwestern China. Canadian Journal of Earth Sciences 42, 287–306.
Long, X., Sun, M., Yuan, C., Xiao, W., Cai, K., 2008. Early Paleozoic sedimentary record of the Chinese Altai: implications for its tectonic evolution. Sedimentary Geology 208, 88–100.
Masters, R.L., Ague, J.J., 2005. Regional-scale fluid flow and element mobility in Barrow's metamorphic zones, Stonehaven, Scotland. Contributions to Mineralogy and Petrology 150, 1–18.
McDonough, W.F., Sun, S.-s., 1995. The composition of the Earth. Chemical Geology 120, 223–254.
McLennan, S.M., Hemming, S., McDaniel, D.K., Hanson, G.N., 1993. Geochemical approaches to sedimentation, provenance, and tectonics. In: Johnson, M.J., Basu, A. (Eds.), Processes Controlling the Composition of Clastic Sediments. Geological Society of America Special Paper 284, pp. 21–40.
Miller, C., Thoni, M., Frank, W., Grasemann, B., Klotzli, U., Guntli, P., Draganits, E., 2001. The early Palaeozoic magmatic event in the Northwest Himalaya, India: source, tectonic setting and age of emplacement. Geological Magazine 138, 237–251.
Miller, N., Alene, M., Sacchi, R., Stern, R.J., Conti, A., Kroner, A., Zippi, G., 2003. Significance of the Tambien group (Tigrai, N. Ethiopia) for Snowball Earth events in the Arabian–Nubian Shield. Precambrian Research 121, 263–283.
Murphy, M., 2007. Isotopic characteristics of the Gurla Mandhata metamorphic core complex: implications for the architecture of the Himalayan orogen. Geology 35, 983–986.
Myrow, P.M., Snell, K.E., Hughes, N.C., Paulsen, T.S., Heim, N.A., Parcha, S.K., 2009. Cambrian depositional history of the Zanskar valley region of the Indian Himalaya: tectonic implications. Journal of Sedimentary Research 76, 364–381.
Myrow, P.M., Thompson, K.R., Hughes, N.C., Paulsen, T.S., Sell, B.K., Parcha, S.K., 2006. Cambrian stratigraphy and depositional history of the northern Indian Himalaya, Spiti Valley, north-central India. Geological Society of America Bulletin 118, 491–510.

Nesbitt, H.W., Young, G.M., 1982. Early Proterozoic climates and plate motions inferred from major element chemistry of lutites. Nature 199, 715–717.
Parrish, R.R., Hodges, K.V., 1996. Isotopic constrains on the age and provenance of the Lesser and Greater Himalayan sequences, Nepalese Himalaya. Geological Society of America Bulletin 108, 904–911.
Paul, S.K., 1998. Geology and tectonics of the Central Crystallines of northeastern Kumaun Himalaya, India. Journal of Nepal Geology Society 18, 151–167.
Pearce, J.A., Cann, J.R., 1971. Ophiolite origin investigated by discriminant analysis using Ti, Zr, and Y. Earth and Planetary Science Letters 12, 339–349.
Pearce, J.A., Cann, J.R., 1973. Tectonic setting of basic volcanic rocks determined using trace element analyses. Earth and Planetary Science Letters 19, 290–300.
Pearce, T.H., Gorman, B.E., Birkett, T.C., 1975. The $TiO_2$–$K_2O$–$P_2O_5$ diagram: a method of discriminating between oceanic and non-oceanic basalts. Earth and Planetary Science Letters 24, 419–426.
Pearce, J.A., 1996. A users guide to basalt discrimination diagrams. In: Wyman, D.A. (Ed.), Trace Element Geochemistry of Volcanic Rocks: Applications for Massive Sulfide Exploration, Geological Association of Canada, Short Course Notes 12, pp. 79–113.
Pogue, K.R., Hylland, M.D., Yeats, R.S., Khattak, W.U., Hussain, A., 1999. Stratigraphic and structural framework of Himalayan foothills, northern Pakistan. In: Macfarlane, A., Sorkhabi, R.B., Quade, J. (Eds.), Himalaya and Tibet: Mountain Roots to Mountain Tops, Geological Society of America Special Paper 328, pp. 257–274.
Richards, A., Argles, T., Harris, N., Parrish, R., Ahmad, T., Darbyshire, F., Draganits, E., 2005. Himalayan architecture constrained by isotopic trasers from clastic sediments. Earth and Planetary Science Letters 236, 773–796.
Robinson, D.M., DeCelles, P.G., Patchett, P.J., Garzione, C.N., 2001. The kinematic evolution of the Nepalese Himalaya interpreted from Nd isotopes. Earth and Planetary Science Letters 192, 507–521.
Roedder, E., 1992. Fluid inclusion evidence for immiscibility in magmatic differentiation. Geochemica et Cosmochemica Acta 56, 5–20.
Rudnick, R.L., 2005. Composition of the continental crust. In: Rudnick, R.L. (Ed.), The Crust. Elsevier, Amsterdam, pp. 1–64.
Scotese, C.R., 1997. PALEOMAP Paleogeographic Atlas, PALEOMAP Progress Report 90 Department of Geology, Univ. of Texas, Arlington, TX.
Shi, X., Yin, J., Jia, C., 1996. Mesozoic to Cenozoic sequence stratigraphy and sea-level changes in the Northern Himalayas, southern Tibet, China. Newsletter of Stratigraphy 33, 15–61.
Slack, J.F., Stevens, P.J., 1994. Clastic metasediments of the Early Proterozoic Broken Hill Group, New South Wales, Australia: geochemistry, provenance, and metallogenic significance. Geochimica et Cosmochimica Acta 58, 3633–3652.
Thakur, V.C., Rawat, B.S., 1992. Geological Map of Western Himalaya, 1:1,000,000.Wadia Institute of Himalayan Geology, Dehradun, India.
Upreti, B.N., Yoshida, M., 2005. Basement history and provenance of the Tethys sediments of the Himalaya: an appraisal based on recent geochronologic and tectonic data. In: The 1st International Conference on the ''Geology of Tethys, 2005'', 12–14 November 2005, Cairo.
Valdiya, K.S., 1995. Proterozoic sedimentation and Pan-African geodynamic development in the Himalaya. Precambrian Research 74, 35–55.
Valdiya, K.S., Paul, S.K., Chandra, T., Bhakuni, S.S., Upadhyay, 1999. Tectonic and lithological characterization of Himadri (Great Himalaya) Between Kali and Yamuna rivers, Central Valley. Himalaya Geology 20, 1–17.
Verma, S.P., 2002. Absence of Cocos plate subduction-related basic volcanism in southern Mexico: a unique case on Earth? Geology 30, 1095–1098.
Verma, S.P., 2006. Extension-related origin of magmas from a garnet-bearing source in the Los Tuxtlas volcanic field, Mexico. International Journal of Earth Sciences 95, 871–901.
Virdi, N.S., 1986. Lithostratigraphy and structure of t he Central Crystallines in the Alaknanda and Dhauliganga valleys of Garhwal, UP. In: Saklani, P.S. (Ed.), Currents Trends in Geology vol. IX, Himalayan Thrust and Associated Rocks, vol. 19, pp. 155-166.
Winchester, J.A., Floyd, P.A., 1976. Geochemical magma type discrimination; application to altered and metamorphosed basic igneous rocks. Earth and Planetary Science Letters 28, 459–469.
Wiesmayr, G., Grasemann, B., 2002. Eohimalayan fold and thrust belt: implications for the geodynamic evolution of the NW-Himalaya (India). Tectonics 21, 1058.
Wiesmayr, G., Grasemann, B., Draganits, E., Frank, W., Fritz, H., Miller, C., 1998, The main pre-Himalayan and Himalayan deformation phases in the Pin valley (Spiti, Tethyan Himalaya, NW India). In: 13th Himalaya – Karakorum – Tibet Workshop, Geological Bulletin of the University of Peshawar Special Issue 31, pp. 212–213.
Willems, H., Zhou, Z., Zhang, B., Grafe, K.-U., 1996. Stratigraphy of the Upper Cretaceous and Lower Tertiary strata in the Tethyan Himalayas of Tibet (Tingri area, China). Geologische Rundschau 85, 723–754.
Windley, B.F., Whitehouse, M.J., Ba-Bttat, M.A.O., 1996. Early Precambrian gneiss terranes and Pan-African island arcs in Yemen: crustal accretion of the eastern Arabian Shield. Geology 24, 131–134.
Yin, A., 2006. Cenozoic tectonic evolution of the Himalayan orogen as constrained by along-strike variation of structural geometry, exhumation history, and foreland sedimentation. Earth-Science Reviews 76, 1–131.
Yin, A., Harrison, T.M., 2000. Geologic evolution of the Himalayan-Tibetan orogen. Annual Reviews of Earth and Planetary Sciences 28, 211–280.
Yin, A., Dubey, C.S., Webb, A.A., Kelty, T.K., Grove, M., Gehrels, G.E., Burgess, W.P., 2010a. Geologic correlation of the Himalayan orogen and Indian craton (part 1): structural geology, U–Pb geochronology, and tectonic evolution of the Shillong Plateau and its neighboring regions in NE India. Geological Society of America Bulletin 122, 336–359.
Yin, A., Dubey, C.S., Kelty, T.K., Webb, A.A., Harrison, T.M., Chou, C.Y., Célérier, J., 2010b. Geologic correlation of the Himalayan orogen and Indian craton (part 2): structural geology, U–Pb geochronology, and tectonic evolution of the Eastern Himalaya. Geological Society of America Bulletin 122, 360–395.
Yoshida, M., 1995. Assembly of East Gondwana during the Grenvillian and its rejuvenation during the Pan-African period. Geological Society of India Memoir 34, 25–45.
Yoshida, M., Upreti, B.N., 2006. Neoproterozoic India within East Gondwana: constraints from recent geochronologic data from Himalaya. Gondwana Research 10, 349–356.
Yoshida, M., Santosh, M., Rajesh, H.M., 2003. Role of Pan-African events in the Circum-East Antarctic Orogen of East Gondwana: a critical review. In: Yoshida, M., Windley, B.F., Dasgupta, S. (Eds.), Proterozoic East Gondwana: Supercontinent Assembly and Breakup. Geological Society of London Special Publication 206, pp. 57–75.